Alexandria Engineering Journal (2021) 60, 3243–3252

HOSTED BY

Alexandria University

Alexandria Engineering Journal

www.elsevier.com/locate/aej
www.sciencedirect.com

Combined effects of thermal radiation and thermophoretic motion on mixed convection boundary layer flow

Amir Abbas [a,*], Muhammad Ashraf [a], Ali Jawad Chamkha [b]

[a] Department of Mathematics, Faculty of Science, University of Sargodha, Sargodha 40100, Pakistan
[b] Mechanical Engineering Department, Prince Muhammad Endowment for Nanoscientist and Technology, Prince Muhammad Bin Fahd University, Al-Khobar 31952, Saudi Arabia

Received 1 December 2019; revised 3 January 2021; accepted 16 January 2021

KEYWORDS

Thermophoretic;
Mixed convection;
Implicit finite difference technique;
Thermal radiation;
Sphere

Abstract The current study is concerned with the investigation of the combined effects of thermophoretic motion and thermal radiation on steady, viscous, incompressible and two-dimensional mixed convection flow of optically dense grey fluid. The governing equations are made dimensionless by using suitable dimensionless variables and further are transformed into a convenient form for a numerical algorithm. The transformed flow model is integrated by using an efficient finite difference methd. Effects of the assorted parameters involved in the flow model such as Prandtl number, mixed convection parameter, modified mixed convection parameter, Schmidt number, radiation parameter, thermophoresis parameter and thermophoretic coefficient on velocity field, temperature distribution, and mass concentration are demonstrated graphically. The numerical results of skin friction, the heat transfer rate and the mass transfer rate under the effect of pertinent parameters are displayed in tabular form.

1. Introduction

The thermophoresis is the phenomenon in which the submicron particles migrate to or from the surface due to the temperature-gradient. The force through which these particles move away or towards the surface is called a thermophoretic force. The velocity gained by these particles during their migration is called thermophoretic velocity. The thermophoresis phenomenon has many applications in industry and engineering fields. Studies concerning the interaction of thermophoresis with mixed convection flow by taking the radiation impacts have augmented greatly in the past years because of its significance in many industrial and engineering processes.

Arpaci [1] discussed laminar natural convection flow over a heated vertical plate considering the impact of thermal radiation. Chen and Mucoglu [2] performed the theoretical analysis to investigate free, forced, and mixed convection flow about a sphere. Their findings exhibit that the velocity profile affected by buoyancy force goes away from the local velocity in free

* Corresponding author.
E-mail address: amirabbas4693@gmail.com (A. Abbas).
Peer review under responsibility of Faculty of Engineering, Alexandria University.

https://doi.org/10.1016/j.aej.2021.01.038

Nomenclature

u, v	Horizontal and normal components of velocity
U_∞ (m/s)	Free stream velocity
v_t	Dimensionless thermophor-etic velocity
k	Thermophoretic coefficient
N_t	Thermophoresis parameter
g (m/s^2)	Gravitational acceleration
T (K)	Fluid temperature in boundary layer
T_∞ (K)	Ambient temperature
T_w (K)	Surface temperature
C (kg/m^3)	Mass concentration in boundary layer
C_∞ (kg/m^3)	Mass concentration in ambient fluid
C_w (kg/m^3)	Surface mass concentration
Re	Reynolds number
Sc	Schmidt number
a	Radius of a sphere
R_d	Radiation parameter
D_m	Mass diffusion coefficient
Gr_t	Grashof number
C_P $(J/kg \cdot K)$	Specific heat at constant pressure
Pr	Prandtl number
Gr_c	Modified Grashof number

Greek symbols

λ_t	Mixed convection para-meter
β_t	Thermal expansion coefficient of temperature
α_m (m/s)	Thermal diffusivity
μ $(Pa \cdot s)$	Dynamic viscosity
ν (m^2/s)	Kinematic viscosity
ρ (kg/m^3)	Fluid density
κ $(W/m \cdot K)$	Thermal conductivity
σ^*	Stefan-Boltzmann constant
β_c	Thermal expansion coefficient of mass concentration
κ^*	Mean absorption coefficient
λ_c	Modified mixed convection parameter

Subscripts

w	Wall conditions
∞	Ambient conditions

stream regime for aiding flow and S-shape for reversing flow. Geoola and Cornish [3] studied steady two-dimensional natural convection flow about a solid sphere. Huang and Chen [4] conducted the analysis on the effect of Prandtl number and surface mass transfer in laminar, viscous, steady, and two-dimensional natural convection flow about the sphere which is maintained at non-uniform temperature. Hossain and Takhar [5] investigated mixed convection flow along a vertical plate whose temperature is kept constant in the presence of radiation effects. Convective flow on vertical cylinder under the action of radiation was examined by Hossain and Rees [6]. The motion of micropolar fluid through a plate which is in motion under the radiation effect has been examined by Raptis [7]. Yih [8] performed computational study of features of natural convection flow along the cylinder held horizontally. They deduced from their study that as buoyancy ratio and transpiration parameters are enhanced, then there is intensification in Sherwood and Nusselt number. Turkyilmazogu et al. [9] examined the absolute ad convective instabilities in compressible boundary layer flow induced along the rotating disk numerically. Abdelkhalk et al. [10] discussed the problem of double diffusivitive heat and mass transfer on vertical porous surface in the in the presence of opposing buoyancy forces analytically and numerically. Selim et al. [11] focused the attention on the study of thermophoresis phenomenon coupled with mixed convection flow over the heated vertical permeable fate plate. The Chamkha and Mudhaf [12] paid the attention on the phenomenon of free convection with radiation due to the magnetic field around the porous surface of a sphere. They concluded that local temperature and concentration of the wall are increased as radiation parameter, Hartmann number, and Prandtl number are increased.

Jordan [13] explored radiative magneto- hydrodynamic time-dependent natural convection flow over permeable vertical surface with the inclusion of dissipation effects. He applied a method of network simulation to determine the numerical solutions of the flow model which provides the solutions of both steady and unsteady state of the problem simultaneously. Chiu et al. [14] primarily focused on combined forced and free convection flow in rectangular ducts under the impacts of radiation. They inferred from their findings that radiation accelerated the temperature and minimized the buoyancy effects. Aydın and Kaya, [15] studied magnetohydrodynamics mixed-convection flow through a permeable plate held vertically in the presence of thermal radiation. Battler [16] made the attempt to review the Blasius and Sakiadis flow with the inclusion of radiation effects. Makinde and Ogulu [17] persuaded radiative magnetohydrodynamic free convection flow along permeable plate due to chemical reaction, thermal radiation, and variable viscosity effects. Natural convection flow through the vertical plate by considering magnetic field, thermal radiation, uniform heat flux of surface effects are considered by Ogulu and Makinde [18]. Turkyilmazogu [19] determined the analytic solutions of boundary layer flow generated due to rotating disk taken as porous equipped with heat transfer. Later, the phenomenon of radiative magnetohydrodynamic mixed convection flow along the plate considered vertically maintained at uniform heat flux in the presence of chemical reaction has been discussed by Makinde [20]. The phenomenon of natural convection with chemical reaction and magnetic field through a vertical permeable surface with the action of radiation and Joule heating attracted the attention of Chamkha et al. [21]. They considered micropolar fluid and solved the system of differential equations with the help of approximating scheme known as finite difference method. Their predictions about their results were that, it can be increased the fluid motion, temperature and skin friction by rising radiation parameter values. Turkyilmazoglu [22] analyzed theoretically

the phenomenon of magnetohydrodyanmics flow in the presence of uniform electric field along a rotating disk. Ashraf et al. [23] examined the radiation effects on magnetohydrodynamic free convection fluctuating flow over a magnetized vertical surface and used finite difference method for numerical solutions of the flow model. Ramzan et al. [24] presented the numerical results of three-dimensional, steady, and laminar flow of viscoselastic nanofluid by taking the Soret and Dufour effects. They used homotopy analysis method for numerical simulation of the governing equations. Makinde et al. [25] took the courage to tackle numerically the heat transfer phenomenon under the action of magnetic field as well as with the consideration of the variable viscosity, thermophoresis and chemical reaction. Khan et al. [26] conducted the theoretical study on the model of nanofluid flow and the heat transfer over a rotating disk by using Buongiono's model. Ashraf et al. [27] proposed the model of mixed-convection flow through tightly coiled curved shape pipe for wide ranges of mixed convection parameter. They deduced that the temperature and the rate of heat transfer is increased by increasing the values of Planck number and Richardson number respectively. Turkyilmazogu [28] proposed the model of unsteady boundary layer flow generated due to vertical rotating disk. Sachin [29] with his co-researchers considered the effects of magnetic field and viscous dissipation on bioconvection flow in nanofluid along the surface of porous sphere embedded in porous medium. The mechanism of radiating and chemically reacting nanofluid along the exponential stretching surface has been investigated by Nayak et al. [30]. Sachin et al. [31] took into account the problem of nanofluid coupled with viscous dissipation and thermal radiation along the three different geometries by using local linearization method. Nayak et al. [32] have paid their attention on three dimensional free convection flow in nanofluid over a stretched surface with the impact of variable magnetic field and thermal radiation.

In the light of the above literature review, it is worthy to mention that, no one has attempted to investigate the heat transfer and fluid flow mechanism about a sphere in the presence of thermophoretic motion and thermal radiation effects. So, motivated by the immense amount of study we interact with the phenomenon of thermophoretic motion and thermal radiation with mixed convection boundary layer flow.

2. Governing equations

Contemplate two-dimensional, laminar, viscous, and optically dense grey fluid flow about a sphere. The surface of a sphere is maintained at uniform temperature T_w. The mass concentration at the surface of a sphere is C_w. The free stream temperature and mass concentration are T_∞ and C_∞ with $T_w > T_\infty$ and $C_w > C_\infty$ respectively. The $\bar{x}$-axis is taken along the surface of a sphere, whereas $\bar{y}$-axis is normal to it. Diagrammatic representation of the fluid flow model and the coordinate system is presented below in Fig. 1. By following [11] the governing dimensionless set of equations is given as below:

$$\frac{\partial(\sin xu)}{\partial x} + \frac{\partial(\sin xv)}{\partial y} = 0, \tag{1}$$

$$u\frac{\partial u}{\partial x} + v\frac{\partial u}{\partial y} = \frac{\partial^2 u}{\partial y^2} + \lambda_t \theta sinx + \lambda_c \phi sinx, \tag{2}$$

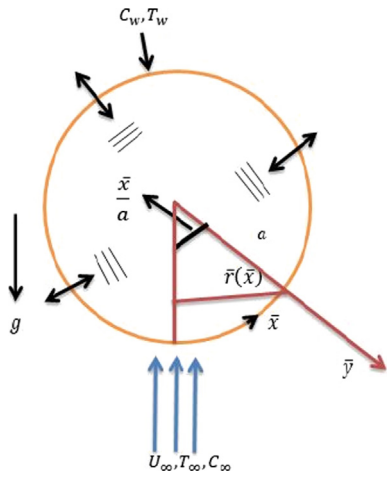

Fig. 1 Coordinate System and Flow Configuration.

$$u\frac{\partial \theta}{\partial x} + v\frac{\partial \theta}{\partial y} = \frac{1}{Pr}\left(1 + \frac{4}{3R_d}\right)\frac{\partial^2 \theta}{\partial y^2} \tag{3}$$

$$u\frac{\partial \phi}{\partial x} + v\frac{\partial \phi}{\partial y} = \frac{1}{Sc}\frac{\partial^2 \phi}{\partial y^2} - \frac{\partial(v_t \phi)}{\partial y}, \tag{4}$$

Here, $Re = U_\infty a/v$, $Gr_t = g\beta_t(T - T_\infty)a^3/v^2$, $Gr_c = g\beta_c(C - C_\infty)a^3/v^2$, $\lambda_t = Gr_t/Re^2$, and $\lambda_c = Gr_c/Re^2$ denote Reynolds number, Grashof number, modified Grashof number mixed convection parameter, and modified mixed convection parameter respectively. The symbols $R_d = \kappa\kappa^*/4\sigma^* T_\infty^3$, $Pr = v/\alpha$, and $Sc = v/D_m$ are adiation parameter, Prandtl number, and Schmidt number respectively. The temperature along the $\bar{x}$-axis is less than along $\bar{y}$-axis in boundary layer flow, hence the themrophoretic velocity is considered along $\bar{y}$-axis. The thermophoretcic velocity appeared in Eq. (4) in non-dimensional form is defined as below

$$v_t = -\frac{k}{\theta + N_t}\frac{\partial \theta}{\partial y},$$

where $k$is thermophoretic coefficient, and $N_t = \frac{\Delta T}{T_\infty}$ is thermophoresis parameter.

Appropriate dimensionless forms of the boundary conditions are

$$\begin{array}{l} u = 0,\ \ v = 0,\ \ \theta = 1,\ \ \phi = 1 \ \text{ at } \ y = 0 \\ u \to 1,\ \ \theta \to 0,\ \ \phi \to 0,\ \ \text{as } \ y \to \infty \end{array}. \tag{5}$$

2.1. Method of solution

Eqs. (1)–(5) are transformed into convenient form for algorithm by using the following the transformation variables

$$u(x,y) = U(X,Y),\ Y = x^{-\frac{1}{2}}y,\ v(x,y) = x^{-\frac{1}{2}}V(X,Y),$$
$$X = x,\ \theta(x,y) = X^{-1}\theta(\mathrm{X},\mathrm{Y}),$$

$$v_t(x,y) = x^{-\frac{1}{2}}V_t(X,Y),\ \phi(x,y) = X^{-1}\phi(\mathrm{X},\mathrm{Y}). \tag{6}$$

The governing conservation Eqs. (1)–(5) take the following form:

$$XUcosX+\left(X\frac{\partial U}{\partial X}-\frac{Y}{2}\frac{\partial U}{\partial Y}+\frac{\partial V}{\partial Y}\right)sinX=0, \tag{7}$$

$$XU\frac{\partial U}{\partial X}+\left(V-\frac{YU}{2}\right)\frac{\partial U}{\partial Y}=\frac{\partial^2 U}{\partial Y^2}+(\lambda_t\theta+\lambda_c\phi)\text{sinX}, \tag{8}$$

$$XU\frac{\partial \theta}{\partial X}+\left(V-\frac{YU}{2}\right)\frac{\partial \theta}{\partial Y}-U\theta=\frac{1}{Pr}\left(1+\frac{4}{3R_d}\right)\frac{\partial^2\theta}{\partial Y^2}, \tag{9}$$

$$XU\frac{\partial \phi}{\partial X}+\left(V-\frac{YU}{2}\right)\frac{\partial \phi}{\partial Y}-U\phi=\frac{1}{Sc}\frac{\partial^2\phi}{\partial Y^2}-\frac{\partial(V_t\phi)}{\partial Y}, \tag{10}$$

where $V_t=-\frac{k}{\theta+\text{XN}_\text{t}}\frac{\partial\theta}{\partial Y}$.

Subject to the boundary conditions are

$$U=0,V=0,\theta=1,\phi=1,\ \text{at}\ \ Y=0$$

$$U\to 1,\theta\to 0,\phi\to 0,\ \text{as}\ \ \text{Y}\to\infty. \tag{11}$$

The finite difference method is applied to approximate the governing momentum, energy and mass equations. The central difference is applied along y-axis, and backward difference along x-axis. After employing the computational technique in Eqs. (7)–(11), we obtain the following general form an algebraic equation

$$A\psi_{i-1,j}+B\psi_{i,j}+C\psi_{i+1,j}=D, \tag{12}$$

where ψ represents the fileds variables U,V,θ, and ϕ with $A,B,C$and D as corresponding coefficients matrices for each unknown variable respectively. The obtained discritized algebraic system of equations is solved by using the Gaussian elimination technique to calculate unknown variables U,θ,and ϕ. Further, the slopes of U,θ, and ϕ designate the mass transfer rate, skin friction, and heat transfer rate respectively.

2.2. Group of stream function formulation

Now we determine the similar solutions of the Eqs. (1)–(4) associated with boundary conditions (5). For this purpose, we transform non-dimensional form of the partial differential equations (1)–(4) along with boundary conditions (5) into a system of ordinary differential equations by using an appropriate group of stream function formulation. In the following similarity transformation variables are given as

$$X=x,\eta=\frac{y}{X^{\frac{1}{2}}},\psi(x,y)=X^{\frac{1}{2}}f(\eta),\theta(x,y)=\theta(\eta),\phi(x,y)=\phi(\eta). \tag{13}$$

where η is similarity variable, ψ is non-dimensional stream function usually taken as $ru=\partial(r\psi)/\partial y$ and $rv=-\partial(r\psi)/\partial x$, $\theta(\eta)$ is the dimensionless temperature profile and $\phi(\eta)$ is the dimensionless mass concentration. Using Eq. (13), the equation of continuity (1) is satisfied automatically and Eqs. (2)–(4) reduce to the following similarity equations

$$f'''+\left(\frac{1}{2}+XcotX\right)ff''+XsinX\theta\lambda_t+XsinX\theta\lambda_t=0 \tag{14}$$

$$\frac{1}{Pr}\left(1+\frac{4}{3R_d}\right)\theta''+\left(\frac{1}{2}+XcotX\right)f\theta'=0 \tag{15}$$

$$\frac{1}{Sc}\phi''+\left(\frac{1}{2}+XcotX\right)f\phi'+\frac{k}{Nt+\theta}\left(\theta'\phi'+\phi\theta''-\frac{\phi\theta'^2}{Nt+\theta}\right)=0. \tag{16}$$

Associated boundary conditions are

$$f=0,f'=0,\theta=1,\phi=1\ \text{at}\ \eta=0,$$

$$f'\to 1,\theta\to 0,\phi\to 0,\ \text{as}\ \eta\to\infty. \tag{17}$$

The transformed thermophoretic velocity is given by

$$V_t=-\frac{k}{\theta+\text{N}_\text{t}}\theta'(0).$$

The transformed system of ordinary differential equations (14)–(16) with boundary conditions (17) are solved by using built-in Numerical Solver BVP4C. Here BVP4C stands for boundary value problem of four order code. The comparison of the solutions of the flow model for the skin friction, the rate of heat transfer, and the rate of mass transfer obtained at the leading edge by FDM and BVP4C is given in Tables 1, and is concluded that results obtained by both schemes are good in agreement which shows the validation of solutions obtained by FDM applied to the primitive form of the partial differential equations.

3. Results and discussion

The present analysis is performed on the combined effects of thermophoretic motion and thermal radiation on mixed convection flow along the surface of a sphere at several circumferential locations. The action of governing parameters such as thermphoresis parameter, mixed convection parameter, radiation parameter, Prandtl number, Schmidt number and thermophoretic coefficient are seen on heat transfer rate and flow characteristics. The set of numerical solutions for fluid velocity, temperature field, and mass concentration along with skin friction, heat transfer rate, and mass transfer rate owing to vary the involved assorted parameters are displayed in graphical as well as tabular representation. Fig. 2(a)–(c) portray the effect of various values of radiation parameter on velocity and temperature fields along with mass concentration respectively at different locations of the surface of a sphere. Graphical results depict that increasing values of radiation parameter results in augmentation of velocity and temperature fields but the reverse behavior is noticed in mass concentration. This may be attributed to the fact that thermal radiation causes the enhancement in the temperature of the fluid flow domain. Moreover, it is observed that the fluid velocity achieves the highest magnitude at $X=\pi/2$ among all the considered positions, on the other hand, temperature and mass concentration obtain such behavior at point $X=\pi$. Fig. 3 (a)–(c) express the behaviors of physical properties mentioned earlier for various values of Prandtl number Pr. It is seen that an intensification in Prandtl number Pr leads to a decrease in velocity profile but an increase in temperature distribution and mass concentration is noticed. It is a noticeable point that velocity gets reduced at position $X=\pi$. Furthermore, it is deduced that maximum fluid velocity is at position $X=\pi/2$ but highest magnitude temperature and mass concentration is at position $X=\pi$. Fig. 4(a)-(c) express the behaviors of

Table 1 Numerical solutions of the skin friction, the rate of heat trasnfer, and the rate of mass transfer obtained by the Finite Difference Method (FDM) and built-in numerical solver boundary value problem of fourth order code (BVP4C) for different values of radiation parameter R_d when $\lambda_t = 1.0$, $\lambda_c = 1.0$, $N_t = 0.5$, Sc = 2.0, $k = 1.0$, and Pr = 0.71 at $X = \pi/2$radian.

R_d	$\left(\frac{\partial U}{\partial Y}\right)_{Y=0}$		$\left(\frac{\partial \theta}{\partial Y}\right)_{Y=0}$		$\left(\frac{\partial \phi}{\partial Y}\right)_{Y=0}$	
	FDM	BVP4C	FDM	BVP4C	FDM	BVP4C
0.1	2.92670	2.92884	0.47019	0.47000	0.47628	0.47932
1.0	3.02741	3.02944	0.36883	0.36961	0.53354	0.53708
2.0	3.07591	3.07838	0.32913	0.32908	0.56242	0.56408
3.0	3.10355	3.10444	0.30728	0.30899	0.57319	0.57825
4.0	3.12013	3.12053	0.29677	0.29702	0.58248	0.58693

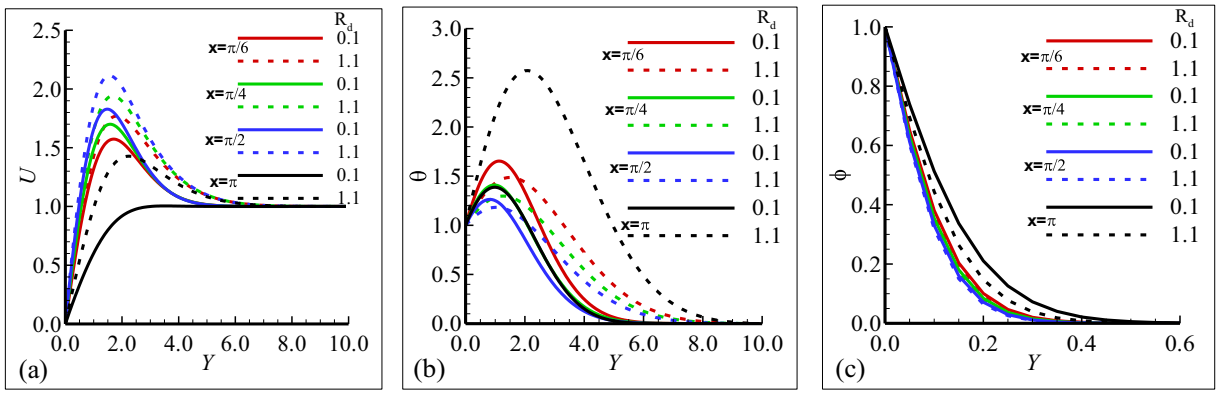

Fig. 2 Plots of (a) velocity profile (b) temperature profile and (c) mass concentration for $R_d = 0.1, 1.1$ when $\lambda_t = 1.1$, $\lambda_c = 1.1$, Pr = 0.71, Sc = 2.0, $N_t = 0.4$, and k = 1.0.

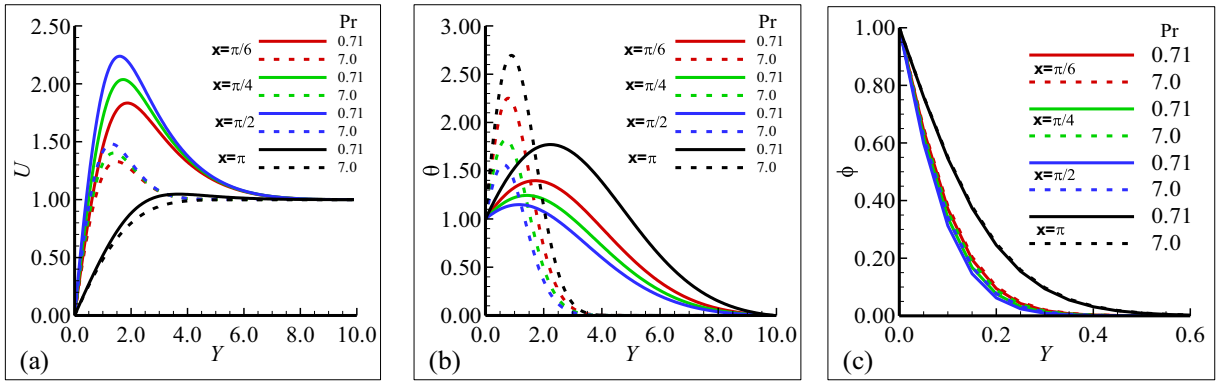

Fig. 3 Plots of (a) velocity profile (b) temperature profile and (c) mass concentration for Pr= 0.71, 7.0 when $\lambda_t = 1.1$, $\lambda_c = 1.1$, $R_d = 2.0$, Sc = 2.0, $N_t = 0.5$, and k = 1.0.

physical quantities such as velocity and temperature fields along with mass concentration for the given values of other parameters at different locations for the imposition of various values of λ_t. It is inferred from Fig. 4(a)–(c) that increasing values of mixed convection parameter λ_t tends to accelerate the fluid velocity with the attenuation in temperature and concentration profiles. It is deduced from these figures that velocity profile gets maximum value at position $X = \frac{\pi}{2}$ but, in contrast temperature distribution and mass concentration attain such behavior at $X = \pi$. The behavior of physical quantities mentioned above is displayed in Fig. 5(a)–(c) at various positions around the sphere for several values of Schmidt number. From the results given in Fig. 5(a)–(c), we can see that an increase in Sc is accompanied by rise in fluid velocity, but reduction in mass and temperature profiles. In addition, velocity profile is maximum at position $X = \frac{\pi}{2}$ but temperature distribution and mass concentration obtain maximum values at circumferential location $X = \pi$.

Fig. 6(a)–(c) presents the effect of $\lambda_c$on velocity and temperature fields along with mass concentration at positions

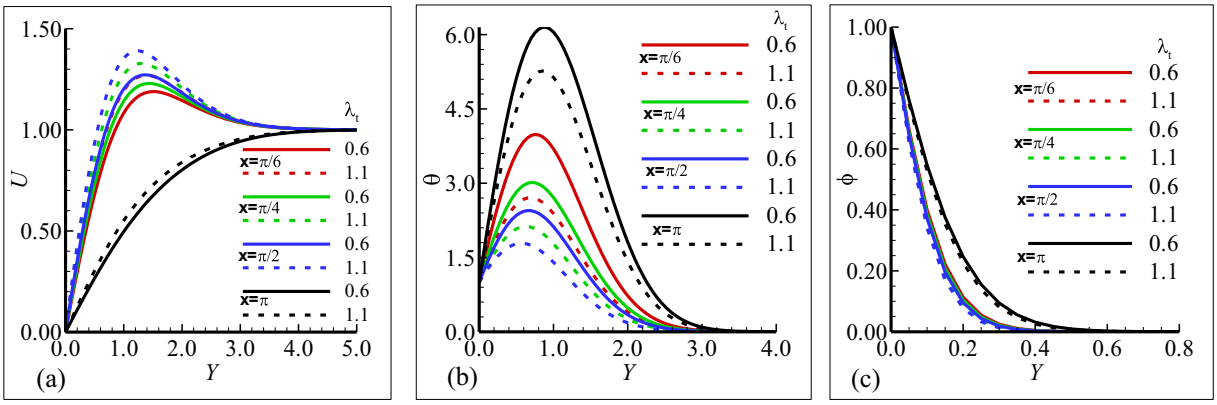

Fig. 4 Plots of (a) velocity profile (b) temperature profile and (c) mass concentration for $\lambda_t = 0.6, 1.1$when $R_d = 1.1$, $\lambda_c = 1.0$, Pr= 7.0, Sc= 2.0, $N_t = 0.6$, and k = 1.0.

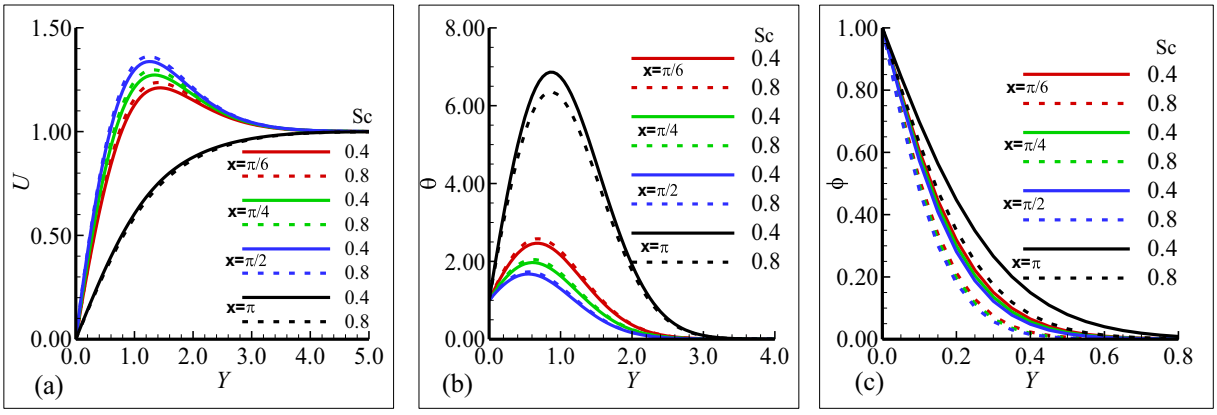

Fig. 5 Plots of (a) velocity profile (b) temperature profile and (c) mass concentration for Sc = 0.4, 0.8 when $\lambda_t = 1.1$, $\lambda_c = 1.1$, Pr = 7.0, $R_d = 1.1$, $N_t = 0.4$, and k = 1.0.

$X = \pi/6, \pi/4, \pi/2, \pi$, for two values of λ_c, keeping the other parameters constant. In these figures, it is shown that increasing values of λ_c implies a reduction in velocity profile at position $X = \pi/6, \pi/4, \pi/2$ but the maximum value for the velocity field is obtained at the position of $X = \pi$. Furthermore, temperature profile decreases at points $X = \pi/6, \pi/4, \pi/2$, but increases at position $X = \pi$. Moreover, it is observed that mass concentration reduces. Graphical interpretation for velocity and temperature fields along with mass concentration for different thermophoresis parameter N_T values at various positions about the surface of a sphere are displayed in Fig. 7 (a)–(c). From these figures, it can be seen that no significant variations have been observed in all considered physical properties by increasing the values of N_t. We can conclude from

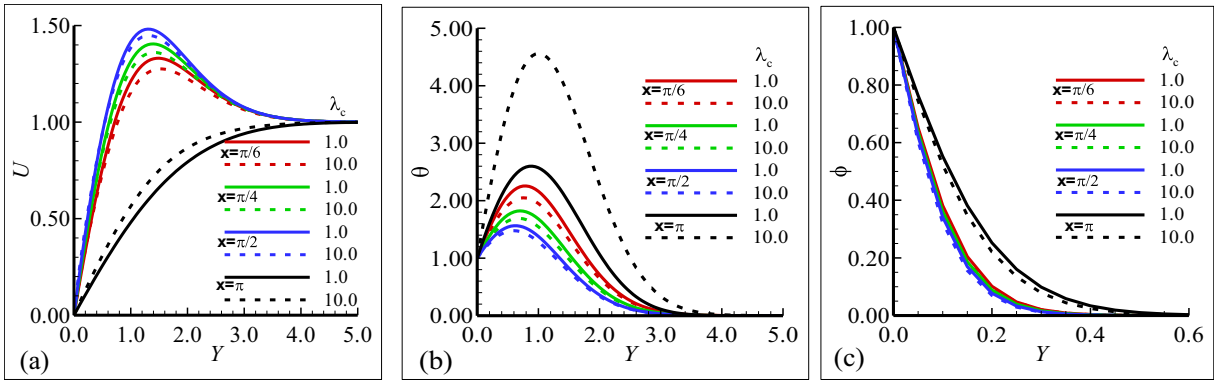

Fig. 6 Plots of (a) velocity profile (b) temperature profile and (c) mass concentration for $\lambda_c = 1.0, 10.0$, when $\lambda_t = 1.1$, $R_d = 2.0$, Pr = 7.0, Sc= 2.0, $N_t = 0.5$, and k = 1.0.

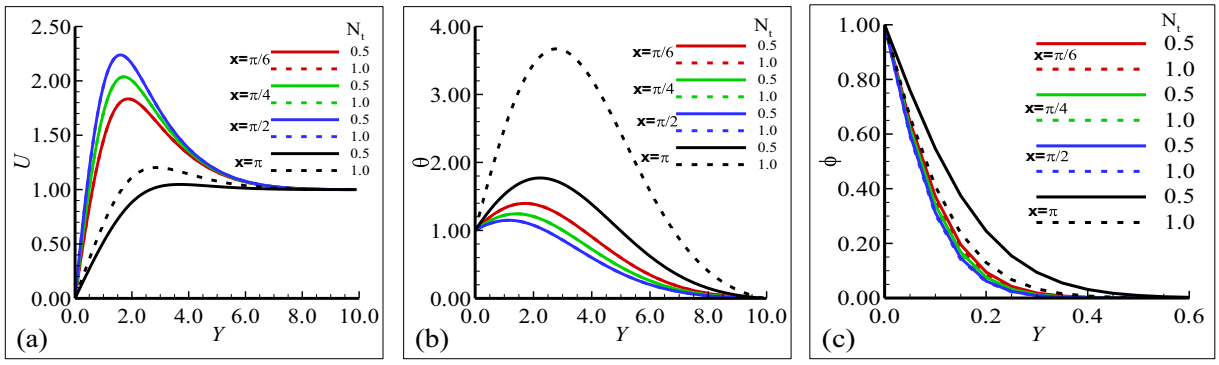

Fig. 7 Plots of (a) velocity profile (b) temperature profile and (c) mass concentration for $N_t = 0.5, 1.0$ when $\lambda_t = 1.1$, $\lambda_c = 1.1$, Pr = 0.71, Sc = 2.0, $R_d = 2.0$, and k = 1.0.

these graphs that velocity and temperature fields rise but mass concentration decreases with prominent difference only at position $X = \pi$. Fig. 8(a)–(c) reflects that higher choice of k causes an increase in velocity and temperature fields but mass concentration is reduced.

Table 1 presents the comparison of the results for the skin friction, the rate of heat transfer, and the rate of mass transfer for different values of the radiation parameter R_d, when the rest of the physical parameters are kept constant at a favorable point $X = \pi/2$ radian. It can be observed that observed that the results of the current problem obtained by FDM and the built-in numerical solver BVP4C seem to be in good agreement. The numerical solutions of the proposed model by FDM were obtained on the entire surface of the flow geometry. On the other side, numerical solutions of the skin friction, the rate of heat transfer and the rate of mass transfer by the built-in numerical solver BVP4C are obtained at the leading edge of the surface of the sphere for the similar form of the equations given in Eqs. (14)–(16) with boundary conditions Eq. (17). Therefore the numerical results obtained by the finite difference method are validated by the built-in numerical solver BVP4C at the leading edge. The comparison of the numerical solutions by both schemes given in the Table 1 endorses the claim that the main numerical method (FDM) chosen in the current study is accurate.

In Table 2, the effect of various values radiation parameter R_d on skin friction, the rate of heat transfer and the the mass transfer rate at different circumferential positions of the surface of a sphere are shown. After sighting at the result for proposed physical properties, it is worthy to express that an increase in radiation parameter R_d causes the intensification in skin friction and the mass transfer rate at the expense of a decrease in the rate of heat transfer. Our findings illuminate that maximum values for the skin friction and the mass transfer rate are obtained at point $X = \pi/2$ but the rate of heat transfer achieves peak magnitude at $X = \pi/4$. For various values of mixed convection parameter $\lambda_t$by taking other parameters constant, the numerical solutions for assumed physical properties are presented in Table 3. It is noticed that as λ_t is raised from 0.6 to 1.1, the skin friction and the mass transfer rate are increased along with the diminishment in the rate of heat transfer. A maximum magnitude for skin friction and the mass transfer rate is seen at point $X = \pi/2$ but in the case of the rate of heat transfer maximum magnitude is observed at location $X = \pi/4$. Table 4 presents the behaviors of assumed material properties for various values of Schmidt number Sc at several positions of the sphere surface. It is noted that skin friction and the mass transfer rate get reduced, on the other side; the rate of heat transfer gets maximized. In Table 5 effects of thermophoresis parameter $N_t = \Delta T/T_\infty$ have been examined. It is deduced that an increase in N_t at various circumferential positions of sphere leads to a reduction in the skin friction but an rise in the heat transfer rate and the mass transfer rate. Table 6 shows the impacts of increasing values of thermophoretic coefficient k. From these results presented in Table 6, it is noted that owing to raise the values of k results

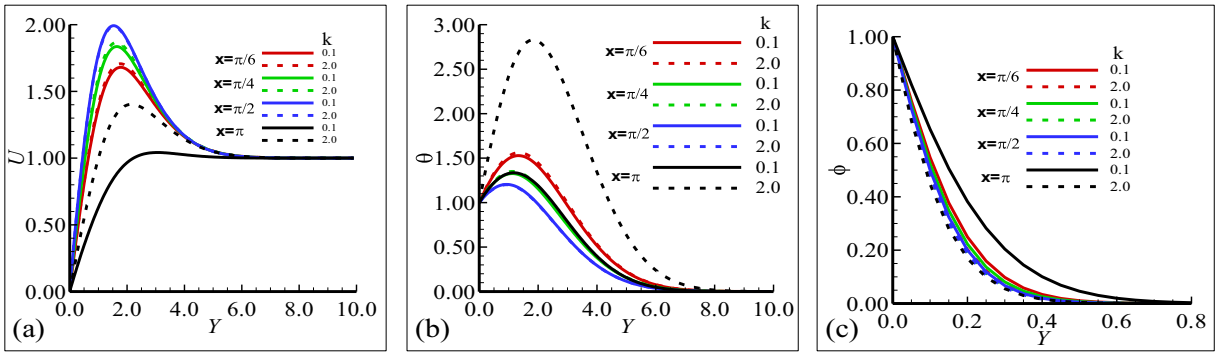

Fig. 8 Plots of (a) velocity profile (b) temperature profile and (c) mass concentration for k = 0.1, 2.0when $\lambda_t = 1.1$, $\lambda_c = 1.1$, Pr = 0.71, Sc = 0.6, $R_d = 0.6$, and $N_t = 2.0$.

Table 2 Numerical solutions of the skin friction, the rate of heat transfer, and the rate rate mass transfer for several values of R_d when $\lambda_t = 1.1$, $\lambda_c = 1.1$, $N_t = 0.4$, Sc $= 2.0$, $k = 1.0$, and Pr$= 0.71$.

X	$\left(\frac{\partial U}{\partial Y}\right)_{Y=0}$		$\left(\frac{\partial \theta}{\partial Y}\right)_{Y=0}$		$\left(\frac{\partial \phi}{\partial Y}\right)_{Y=0}$	
	$R_d = 0.1$	$R_d = 1.1$	$R_d = 0.1$	$R_d = 1.1$	$R_d = 0.1$	$R_d = 1.1$
$\pi/6$	2.03983	2.12816	0.94670	0.57034	0.37895	0.44799
$\pi/4$	2.47647	2.61447	0.70285	0.42245	0.52161	0.59891
$\pi/2$	2.94238	3.13261	0.53525	0.31783	0.64543	0.72913
π	0.57487	1.26779	−0.41769	1.25722	−1.40916	0.02432

Table 3 Numerical solutions of the skin friction, the rate of heat transfer, and the rate rate mass transfer for several values of λ_t when $R_d = 1.1$, $\lambda_c = 1.0$, $N_t = 0.6$, Sc$= 2.0$, $k = 1.0$, and Pr$= 7.0$.

X	$\left(\frac{\partial U}{\partial Y}\right)_{Y=0}$		$\left(\frac{\partial \theta}{\partial Y}\right)_{Y=0}$		$\left(\frac{\partial \phi}{\partial Y}\right)_{Y=0}$	
	$\lambda_t = 0.6$	$\lambda_t = 1.1$	$\lambda_t = 0.6$	$\lambda_t = 1.1$	$\lambda_t = 0.6$	$\lambda_t = 1.1$
$\pi/6$	1.65689	1.92757	3.59158	2.86681	0.06615	0.22088
$\pi/4$	1.93361	2.26942	2.64866	2.12042	0.19445	0.34618
$\pi/2$	2.23234	2.63754	2.06337	1.64349	0.30665	0.45680
π	0.45237	0.45625	0.04097	0.09461	−1.38045	−1.41867

Table 4 Numerical solutions of the skin friction, the rate of heat transfer, and the rate rate mass transfer for several values of Sc when $R_d = 1.1$, $\lambda_c = 1.1$, $N_t = 0.4$, $\lambda_t = 1.1$, $k = 1.0$, and Pr $= 7.0$.

X	$\left(\frac{\partial U}{\partial Y}\right)_{Y=0}$		$\left(\frac{\partial \theta}{\partial Y}\right)_{Y=0}$		$\left(\frac{\partial \phi}{\partial Y}\right)_{Y=0}$	
	$Sc = 0.4$	$Sc = 0.8$	$Sc = 0.4$	$Sc = 0.8$	$Sc = 0.4$	$Sc = 0.8$
$\pi/6$	2.00558	1.94481	1.61318	2.03060	0.30663	0.30660
$\pi/4$	2.43949	2.34261	1.14436	1.47669	0.36558	0.38744
$\pi/2$	2.90579	2.76677	0.82856	1.11180	0.41881	0.45991
π	0.42421	0.43994	0.80678	0.41357	−0.08484	−0.33222

Table 5 Numerical solutions of the skin friction, the rate of heat transfer, and the rate rate mass transfer for several values of N_t when $R_d = 2.0$, $\lambda_t = 1.1$, $\lambda_c = 1.1$, Sc $= 2.0$, $k = 1.0$, and Pr $= 0.71$.

X	$\left(\frac{\partial U}{\partial Y}\right)_{Y=0}$		$\left(\frac{\partial \theta}{\partial Y}\right)_{Y=0}$		$\left(\frac{\partial \phi}{\partial Y}\right)_{Y=0}$	
	$N_t = 0.5$	$N_t = 1.0$	$N_t = 0.5$	$N_t = 1.0$	$N_t = 0.5$	$N_t = 1.0$
$\pi/6$	2.14887	2.10197	0.41992	0.42340	0.46428	0.91738
$\pi/4$	2.66645	2.63628	0.3148	0.31573	0.62466	0.90933
$\pi/2$	3.21630	3.20043	0.23727	0.23720	0.76117	0.94513
π	−0.61841	0.14612	−0.90433	−1.46610	−0.15826	−0.33307

in a reduction in skin friction and the mass transfer rate along with intensification in the rate of heat transfer. Table 7 illuminates the effect of Pr on already mentioned properties in previous tables. It shows that an increase in Pr leads to a rise in skin friction and the rate of heat transfer but a decrease in the mass transfer rate at position $X = \pi$.It is interesting to note that no significant variations have noticed on properties at other considered positions.

Table 6 Numerical solutions of the skin friction, the rate of heat transfer, and the rate rate mass transfer for several values of k when $R_d = 0.6$, $\lambda_t = 1.1$, $\lambda_c = 1.1$, Sc= 0.6, $N_t = 2.0$, and Pr = 0.71.

X	$\left(\frac{\partial U}{\partial Y}\right)_{Y=0}$		$\left(\frac{\partial \theta}{\partial Y}\right)_{Y=0}$		$\left(\frac{\partial \phi}{\partial Y}\right)_{Y=0}$	
	$k = 0.1$	$k = 2.0$	$k = 0.1$	$k = 2.0$	$k = 0.1$	$k = 2.0$
$\pi/6$	0.37983	0.37527	0.74533	0.90341	0.30263	0.06164
$\pi/4$	0.37983	0.37527	0.14533	0.9034	0.30263	0.06164
$\pi/2$	3.26393	3.45320	0.30970	0.22388	−0.57264	−0.57120
π	0.37983	0.37527	−0.74533	−0.90341	0.30263	0.06164

Table 7 Numerical solutions of the skin friction, the rate of heat transfer, and the rate rate mass transfer for several values of Pr when $R_d = 2.0$, $\lambda_t = 1.1$, $\lambda_c = 1.1$, Sc = 2.0, $N_t = 0.5$, and $k = 1.0$.

X	$\left(\frac{\partial U}{\partial Y}\right)_{Y=0}$		$\left(\frac{\partial \theta}{\partial Y}\right)_{Y=0}$		$\left(\frac{\partial \phi}{\partial Y}\right)_{Y=0}$	
	$Pr = 0.71$	$Pr = 7.0$	$Pr = 0.71$	$Pr = 7.0$	$Pr = 0.71$	$Pr = 7.0$
$\pi/6$	2.15115	2.15115	0.41986	0.41986	−0.44768	−0.44768
$\pi/4$	2.66902	2.66902	0.31477	0.31477	−0.60992	−0.60992
$\pi/2$	3.21921	3.21921	0.23721	0.23721	−0.74741	−0.74741
π	−0.62939	0.74821	−0.91522	1.76364	0.12329	−0.17287

4. Conclusion

In the present study the mixed convection flow around the surface of a sphere subject to the combined effects of thremophoretic motion and thermal radiation are studied numerically. An efficient finite difference method on the governing boundary layer equations is applied for numerical solutions. Our computations have been carried out for wide ranges of various pertinent parameters to examine the solution in flow regime. We summarize our findings as below:

- It can be seen that by increasing the values of $R_d, \lambda_t, \mathrm{Sc}, \lambda_c, N_t$ and k the vlocity profile increases but decreases due to increasing values of Pr.
- It can be observed that by rising the values of R_d,Pr, N_t and k the velocity profile increases but decreases due to increasing values of $\lambda_t, \mathrm{Sc}, \lambda_{c,}$.
- The mass concentration increases owing to increase the values of Pr, and N_t but decreasing attitude is seen with the augmentaion in R_d, λ_t, Sc, λ_c and k.
- In tabular results it can be observed that increasing values of R_d, λ_t and Pr lead to enhence the values of the skin friction and on the other hand, decreasing behavior is found for the rising values of Sc, N_t and k.
- The rate of heat transfer is increased by augmenting the values of Sc, N_t, k, and Pr but decreased for the case of R_d and λ_t.
- The rate of mass transfer is enhanced by raising the values of R_d, λ_t, Sc, and N_t but reduced when k and Pr are intensified.
- At the end the results of the skin friction, the rate of heat transfer, and the rate of mass transfer are compared in tabular form for the different values of radiation parameter R_d obtained from built-in numerical solver BVP4C and finite difference method (FDM). The numerical solutions determined by both schemes show the good agreement which validates the main proposed scheme FDM.

Declaration of Competing Interest

The authors declare that they have no known competing financial interests or personal relationships that could have appeared to influence the work reported in this paper.

References

[1] V.S. Arpaci, Effect of thermal radiation on the laminar free convection from a heated vertical plate, Int. J. Heat Mass Transf. 11 (1968) 871–881.

[2] T.S. Chen, A. Mucoglu, Analysis of mixed forced and free convection about a sphere, Int. J. Heat Mass Transf. 2 (1977) 867–875.

[3] F. Geoola, A.R.H. Cornish, Numerical solution of steady-state free convective heat transfer from a solid sphere, Int. J. Heat Mass Transf. 21 (1981) 369–1379.

[4] M. Huang, G.G. Chen, Laminar free convection from a sphere with blowing and suction, J. Heat Transf. (Trans. ASME (Am. Soc. Mech. Engineers) Ser. C (United States) 109 (1987) 529–532.

[5] M.A. Hossain, H.S. Takhar, Radiation effect on mixed convection along a vertical plate with uniform surface temperature, Heat Mass Transf. 31 (1996) 243–244.

[6] M.A. Hossain, D.A. Rees, Radiation-conduction interaction on mixed convection flow along a slender vertical cylinder, J. Thermophys. Heat Transf. 12 (1998) 611–614.

[7] A. Raptis, Flow of a micropolar fluid past a continuously moving plate by the presence of radiation, Int. J. Heat Mass Transf. 18 (1998) 2865–2866.

[8] K.A. Yih, Coupled heat and mass transfer by natural convection adjacent to a permeable horizontal cylinder in a saturated porous medium, Int. Commun. Heat Mass Transfer 26 (1999) 431–440.

[9] M. Turkyilmazoglu, J.W. Cole, J.S.B. Gajjar, Absolute and convective instabilities in the compressible boundary layer on a rotating disk, Theor. Comput. Fluid Dyn. 14 (2000) 21–37.

[10] A. Amahmid, M. Hasnaoui, S. Douamna, Analytical and numerical study of double diffusive parallel flow induced in a

vertical porous layer subjected to constant heat and mass fluxes, J. Mech. Eng. 47 (2001) 501–505.
[11] A. Selim, M.A. Hossain, D.A.S. Rees, The effect of surface mass transfer on mixed convection flow past a heated vertical flat permeable plate with thermophoresis, Int. J. Therm. Sci. 42 (2003) 973–982.
[12] A.J. Chamkha, A. Al-Mudhaf, Simultaneous heat and mass transfer from a permeable sphere at uniform heat and mass fluxes with magnetic field and radiation effects, Numer. Heat Transfer, Part A 46 (2004) 181–198.
[13] J.Z. Jordán, Network simulation method applied to radiation and viscous dissipation effects on MHD unsteady free convection over vertical porous plate, Appl. Math. Model. 31 (2007) 2019–2033.
[14] H.C. Chiu, J.H. Jang, W.M. Yan, Mixed convection heat transfer in horizontal rectangular ducts with radiation effects, Int. J. Heat Mass Transf. 50 (2007) 2874–2882.
[15] O. Aydın, A. Kaya, Radiation effect on MHD mixed convection flow about a permeable vertical plate, Heat Mass Transf. 45 (2008) 239–246.
[16] R.C. Bataller, Radiation effects for the Blasius and Sakiadis flows with a convective surface boundary condition, Appl. Math. Comput. 206 (2008) 832–840.
[17] O.D. Makinde, A. Ogulu, The effect of thermal radiation on the heat and mass transfer flow of a variable viscosity fluid past a vertical porous plate permeatedby a transverse magnetic field, Chem. Eng. Commun. 195 (2008) 1575–1584.
[18] A. Ogulu, O.D. Makinde, Unsteady hydromagnetic free convection flow of a dissipative and radiating fluid past a vertical plate with constant heat flux, Chem. Eng. Commun. 196 (2008) 454–462.
[19] M. Turkyilmazoglu, Purely analytic solutions of the compressible boundary layer flow due to a porous rotating disk with heat transfer, Phys. Fluids 21 (2009), https://doi.org/10.1063/1.3249752.
[20] O.D. Makinde, MHD mixed-convection interaction with thermal radiation and nth order chemical reaction past a vertical porous plate embedded in a porous medium, Chem. Eng. Commun. 198 (2010) 590–608.
[21] A.J. Chamkha, R.A. Mohamed, S.E. Ahmed, Unsteady MHD natural convection from a heated vertical porous plate in a micropolar fluid with Joule heating, chemicalreaction and radiation effects, Meccanica 46 (2011) 399–411.
[22] M. Turkyilmazoglu, Effects of uniform radial electric field on the MHD heat and fluid flow due to a rotating disk, Int. J. Eng. Sci. 51 (2012) 233–240.
[23] M. Ashraf, S. Asgharand, M.A. Hossain, Fluctuating hydromagnetic natural convection flow past a magnetized vertical surface in the presence of thermal radiation, Therm. Sci. 16 (2012) 1081–1096.
[24] M. Ramzan, S. Inam, S.A. Shehzad, Three dimensional boundary layer flow of a viscoelastic nanofluid with Soret and Dufour effects, Alex. Eng. J. 55 (2016) 311–319.
[25] O.D. Makinde, W.A. Khan, J.R. Culham, MHD variable viscosity reacting flow over a convectively heated plate in a porous medium with thermophoresis and radiative heat transfer, Int. J. Heat Mass Transf. 93 (2016) 595–604.
[26] Khan, J. Ahmad, M. Mustafa, T. Hayat, M. Turkyilmazoglu, A. Alsaedi, Numerical study of nanofluid flow and heat transfer over a rotating disk using Buongiorno's model, Int. J. Numer. Meth. Heat Fluid Flow (2017), https://doi.org/10.1108/HFF-08-2015-0328.
[27] M. Ashraf, R. Yasmeen, M. Ahmad, Thermal radiation mixed convection boundary-layer flow in tightly coiled curved pipe for large Richardson number, Therm. Sci. 22 (2018) 147–156.
[28] M. Turkyilmazoglu, Fluid flow and heat transfer over a rotating and vertically moving disk, Phys. Fluids 30 (2018) 063605.
[29] S. Sachin, S.S. Motsa, P. Sibanda, Magnetic field and viscous dissipation effect on bioconvection in a permeable sphere embedded in a porous medium with a nanofluid containing gyrotactic micro-organisms, Heat Transfer—Asian Res. 47 (2018) 718–734.
[30] M.K. Nayak, S. Shaw, O.D. Makinde, Chemically reacting and radiating nanofluid flow past an exponentially stretching sheet in a porous medium, Indian J. Pure Appl. Phys. (IJPAP) 56 (2018) 773–786.
[31] S. Sachin, S.S. Motsa, P. Sibanda, Nanofluid flow over three different geometries under viscous dissipation and thermal radiation using the local linearization method, Heat Transfer—Asian Res. 48 (2019) 2370–2386.
[32] M.K. Nayak, S. Shaw, A.J. Chamkha, 3D MHD free convective stretched flow of a radiative nanofluid inspired by variable magnetic field, Arab. J. Sci. Eng. 44 (2019) 1269–1282.